Transcriptome Analysis Based on Lr19-Virulent Mutants Strain Provides Clues for the Pathogenicity-Related Genes and Effectors of Puccinia Triticina

Wenyue Wu
Hebei Agricultural University
Fan Fan
Hebei Agricultural University
Fei Wang
Hebei Agricultural University
Zhongchi Cui
Hebei Agricultural University
Xinkang Sun
Hebei Agricultural University
Zhen Qin
Hebei Agricultural University
Binbin Peng
Hebei Agricultural University
Daqun Liu
Hebei Agricultural University
Dianping Di
Hebei Agricultural University
Haiyan Wang (ndwanghaiyan@163.com)
Hebei Agricultural University

Research article

Keywords: Wheat leaf rust, mutation, RNA-seq, AvrLr19, effector candidates

Posted Date: September 4th, 2020

DOI: https://doi.org/10.21203/rs.3.rs-62330/v1

Abstract

Background: Wheat leaf rust caused by *Puccinia triticina* (*Pt*) remains one of the most destructive diseases of common wheat worldwide. Cultivating resistant cultivars is an effective way to control this disease, but race-specific resistance can be overcome quickly due to the rapid evolution of *Pt* populations. The critical to control wheat leaf rust is to understand the pathogenicity mechanisms of *Pt*.

Results: In this study, the spores of the *Pt* race PHNT (wheat leaf rust resistance gene *Lr19*-avirulent isolate) were mutagenized with ethyl methanesulfonate (EMS) and two *Pt Lr19*-virulent mutants named M1 and M2 were isolated, suggesting that they carry mutations affecting the *Lr19*-specific avirulent factor. RNA sequencing was performed on samples collected from the wheat cultivars Chinese Spring and TcLr19 that were infected by wild-type (WT) PHNT and the two *Lr19*-virulent mutant isolates at 14 days post-inoculation (dpi). The assembled transcriptome data were compared to the reference genome "*Pt* 1-1 BBBD Race 1." A total of 216 differentially expressed genes (DEGs) were found from three different sample comparisons including M1-vs-WT, M2-vs-WT, and M1-vs-M2. Of these DEGs, 29 common DEGs were shared between M1-vs-WT and M2-vs-WT comparisons. Among the 216 DEGs encoding proteins, 30 were predicted to be effector candidates. Then 6 effector candidates (PTTG_27844, PTTG_05290, PTTG_27401, PTTG_27224, PTTG_26282, PTTG_25521) were verified that these genes were differentially expressed during *Pt* infection by quantitative real-time PCR (qRT-PCR) and were validated on tobacco, and the results showed that PTTG_27401 could inhibit progress of cell death (PCD) induced by BAX.

Conclusions: Our results showed that a large number of genes participate in the interaction between *Pt* and TcLr19, which will provide valuable resources for the identification and targeting of *AvrLr19* effector candidates and pathogenesis-related genes. Furthermore, our analyses are of great significance to reveal the pathogenesis of *Pt*.

Background

Wheat leaf rust caused by *Puccinia triticina* (*Pt*) is one of the most common and severe diseases in the wheat-growing regions worldwide. The yield losses of wheat infected with *Pt* ranges from 5% − 15% and the yield of wheat infected with leaf rust at the seedling stage can be reduced by 50% or even more [1]. Considering the impacts of global climate change, temperature and humidity conditions may be more suitable for the proliferation and epidemic of *Pt* in the future which will further deleteriously impact wheat yields. Control of leaf rust mainly relies on the fungicide application and deployment of cultivars carrying resistance genes. Genetic resistance is the most effective, environmentally safe, and economically feasible approach to reduce the damage caused by *Pt*. However, monoculture of select resistant varieties leads to the host selection pressures that drive *Pt* evolution and promote the continuous emergence of new toxic races, which often leads to the decline of wheat resistant varieties after several years of planting.

To date, over 80 genes conferring leaf rust resistance derived from *Triticum aestivum* wheat cultivars, wild wheat, grass species, and durum wheat have been identified and designated as *Lr1* to *Lr79* [2]. Among them, only *Lr9*, *Lr19*, *Lr24*, *Lr34*, *Lr37*, *Lr38*, *Lr46*, *Lr47*, *Lr51*, *Lr53*, and *Lr68* confer effective resistance to leaf rust currently. *Lr19* is derived from the grass *Agropyron elongatum* and was transferred to the long arm of wheat chromosome 7D [3]. The wheat cultivar carrying *Lr19* is still effective against all *Pt* races in Asia, Australia, Canada, and Europe, and resistance is expressed during the whole growth period [4, 5]. Therefore, *Lr19* holds the potential to be deployed in combination with other *Lr* genes in the field to confer durable resistance against leaf rust worldwide [4, 6]. It has

been reported that *Lr19* is associated with increased grain yield, which promotes it as an important gene for wheat breeding against *Pt*-mediate yield losses [7]. To prevent *Lr19* from being out-competed by newly emergent virulent races, cloning avirulent gene *AvrLr19* that can be recognized by wheat leaf rust resistance gene *Lr19*, determining the molecular mechanism of *AvrLr19* and *Lr19* interactions, and monitoring the natural *Pt* population changes in response to *AvrLr19-Lr19* resistance are key to enable the long-term deployment of *Lr19* in leaf rust-resistant wheat varieties. At present, there is no virulent strain of *Lr19* in the field, which not only benefits the use of *Lr19* but also restricts the development of *AvrLr19*.

Mutation is the most important avenue for creating new rust races and genotypes. Ethyl methanesulfonate (EMS) is an alkylating chemical mutagen that generates single nucleotide polymorphisms (SNPs) and insertions and deletions (Indels), resulting in amino acid sequence variation, and finally leads to phenotype changes that can be selected upon. Mutagenesis integrated with genomic sequencing is an efficient way to study the relationships between phenotypic traits and associated genotypes, leading to the identification of fungal effectors or *Avr* genes. For example, Salcedo *et al.* obtained stripe rust mutants through EMS-induced mutation and performed genome sequencing to obtain *AvrSr35* candidate genes, and then verified the candidate genes through co-expression of *AvrSr35* and its corresponding resistance gene in tobacco and wheat to trigger cell death [8]. Li *et al*. screened 30 mutant variants from the least virulent isolate generated by EMS mutagenesis and candidates *Avr* genes were determined by sequencing [9]. Transcriptomics has proven to be an instrumental molecular tool to help identify virulence effectors and *Avr* genes [10–12]. As the host and pathogen interact in a battle for supremacy, the underlying transcriptional regulation of gene expression in the plant and pathogen provides clues to their defense and virulence mechanisms, respectively [13].

The gene to gene hypothesis proposed by Flor indicates that only the host with an “R gene” is resistant to the homologous *Avr* gene in pathogens [14]. Jone proposed the famous “ZigZag” model in 2006 to analyze the molecular mechanism of interaction between plants and their pathogens [15]. In order to inhibit plant defense responses, pathogens secrete a series of effector proteins through the haustorium to interfere with or ablate the plant defense response, so as to meet their own growth needs. In recent years, with the continuous improvement of sequencing technology and the reduction of sequencing costs, and the development and application of prediction software such as SigalP [16], TargetP [17], TMHMM [18], PredGPI [19] and Pfam [20] have improved the screening efficiency of candidate *Avr* genes of rust. To date, a handful of *Avr* genes have been identified in rust pathogens, including *AvrL567*, *AvrP123*, *AvrP4*, *AvrM*, *AvrL2*, and *AvrM14* from the flax rust pathogen [21], as well as *RTP1* in bean rust [22], and *PGTAUSPE10–1* from wheat stem rust [23]. At the end of 2017, two articles reported the successful cloning of the *Avr* genes *AvrSr35* [8] and *AvrSr50* [24] of wheat stem rust, and preliminarily revealed their interaction with corresponding resistance genes. Some effector candidates for *Lr26*, *Lr9*, and *Lr24* materials were obtained from *Pt* [25] and 20 effector candidates of *Lr20* [26], but their biological functions have not been determined, so, no known *Avr* genes have been identified in *Pt* so far.

In this study, we aim to use an EMS mutagenized *Pt* race PHNT to obtain *Lr19*-virulent mutants, and identify differentially expressed genes (DEGs) associated with the *Pt* infection. Our results provide resources for identification of *AvrLr19* candidates and pathogenicity-related genes, and lay a foundation for revealing the pathogenic mechanism of *Pt*.

Results

Lr19 triggers a resistance response at early stages of infection

Leaf rust resistance conferred by *Lr19* is best expressed in all stages of the wheat plant and culminates in a hypersensitive response (HR) at the infection site which is also known as race-specific resistance [5]. In order to confirm the recognition between *Lr19* and its respective *Avr* gene in the *Lr19*-avirulent *Pt* race PHNT, the phenotype and histopathology examination of *Pt*-infected leaf tissues from resistant TcLr19 (*Lr19*+) and susceptible Chinese Spring *(Lr19*–) wheat lines were analyzed. Compared to Chinese Spring *(Lr19*–) wheat lines, the development of fungal infection hyphae (stained blue) stopped before the formation of a haustorium, the structure with which the fungus extracts nutrients from its host plant, in the resistant wheat line TcLr19 (*Lr19*+). Imaging at 2 dpi revealed fungal growth in susceptible Chines Spring but no further fungal growth in TcLr19, the dead host cells in TcLr19 were stained green, and no dead cells were revealed in Chinese Spring (Fig. 1). This early immune response is consistent with pronounced HR symptoms and suggested early expression of a fungal gene recognized by *Lr19*, which demonstrated that *Lr19* triggers a resistance response at the early stages of infection.

Lr19-virulent mutants were obtained and confirmed

The *Lr19*-avirulent *Pt* race PHNT was used to create *Lr19*-virulent mutants via EMS mutagenesis. The germination rate of PHNT spores under different EMS concentrations was calculated, and the results showed that the germination rate of spores was 50% at an EMS concentration of 0.005 M (Fig. 2A). Two *Pt* mutants virulent to the *Lr19* allele were isolated, named M1 and M2, suggesting that they carried *Lr19*-specific *Avr* factor (Fig. 2B). Confocal microscopy of wheat leaves from the compatible Chinese Spring cultivar infected with the wild-type (WT) and mutant *Pt* strains was performed to investigate the effect of the *AvrLr19* gene mutations on pathogen virulence. In order to ensure the reliability of experimental materials of TcLr19, molecular markers of *Lr19* [27] were used to detect the existence of *Lr19* (Fig. 2C). To validate that only *Lr19*-virulence was affected by the EMS mutagenesis, M1 and M2 were analyzed by infecting a standard full set of near-isogenic lines that carry different *Lr* genes, with the WT PHNT race inoculated as controls (Fig. 2D, Supplementary Table S1). This panel is broadly used for quick pathotyping of unknown *Pt* isolates using a standard 4-letter code. Only TcLr19 inoculated with M1 and M2 demonstrated a change from resistant ('0') to susceptible ('3 +'), while the susceptibility of other near-isogenic lines remained unchanged, indicating that *AvrLr19* was altered in M1 and M2 alleles and that *Lr19*-virulent mutant strains were successfully obtained.

RNA-seq analyses display the information of *Pt* race PHNT and mutants

To characterize the DEGs between Chinese Spring-*Pt* and TcLr19-*Pt* mutants during infection, RNA-seq of TcLr19 inoculated with different *Pt* strains were performed. Following inoculation and incubation, leaves with obvious phenotypes were harvested, then the total RNA was extracted from M1, M2, and WT (Fig. 3A) and was used for RNA-seq cDNA library construction. Quality statistics of sequencing data and the percentages of reads for each sample were mapped to the *Pt* BBBD race reference genome (Supplementary Table S2 and Table S3**)**. The percentage of reads that aligned to the *Pt* reference in M1, M2, and WT are shown in Fig. 3B, respectively. The proportion of reads aligning to the wheat reference Chinese Spring was higher in WT than that in the mutants (Fig. 3B). Based on the density plot (Fig. 3C), box-whisker plot (Supplementary Figure S1A), and the expected number of fragments per kilobase of transcript sequence per million base pairs (FPKM) expression distribution plot (Supplementary Figure S1B) of gene expression levels, it is clear that the expression level of protein-coding genes in each sample is highly similar. Variability among the samples was determined by preparing a principal

component analysis (PCA) (Supplementary Figure S1C). PCA displayed a clear distinction between the transcriptomes of mutant and WT strains.

DEGs were characterized in different combinations

In order to understand the overall distribution of DEGs, volcano maps of DEGs were prepared (Supplementary Figure S2A). The cluster diagram of sample to sample distance matrix was prepared for DEGs to calculate the direct correlation of samples (Supplementary Figure S2B). From the comparison made between M1 and WT (M1-vs-WT), a total number of 168 DEGs were obtained, 74 of which were up-regulated and 94 of which were down-regulated. From the comparison made between M2 and WT (M2-vs-WT), 76 DEGs were obtained, 45 of which were up-regulated and 31 of which were down-regulated. From the comparison made between M1 and M2 (M1-vs-M2), 4 DEGs were obtained, 2 of which were up-regulated and 2 of which were down-regulated (Fig. 4A). Similar DEGs found among the comparisons were shown in a Venn diagram (Fig. 4B). Finally, a total of 216 genes were identified as differentially expressed.

To understand the roles of various biological processes and pathways throughout the infection process, we analyzed Gene Ontology (GO) and Kyoto Encyclopedia of Genes and Genomes (KEGG) enrichment of the 216 DEGs. GO analysis was performed to classify the 216 DEGs into 3 major biological categories. The 216 DEGs belonged to 18 classes in the biological process category, 11 classes in the cellular component category, and 7 classes in the molecular function category (Fig. 5). Among the 216 DEGs, 31 genes are enriched in terms of metabolic processes, 32 genes are enriched in terms of the cell, and 32 genes are enriched in terms of catalytic activity. Through the analysis of KEGG enrichment, we explored the main biochemical metabolic pathways and signal transduction pathways involved in DEGs. The results show that these DEGs are distributed among 10 pathways (Table 1).

Table 1
Results of KEGG analysis of DEGs between M1-vs-WT and M2-vs-WT.

Class	No. of DEGs (M1-vs-WT)	No. of DEGs (M2-vs-WT)
Signal transduction	1	1
Membrane transport	1	-
Translation	1	-
Metabolism of cofactors and vitamins	1	-
Lipid metabolism	4	3
Glycan biosynthesis and metabolism	3	2
Energy metabolism	1	1
Carbohydrate metabolism	9	2
Biosynthesis of other secondary metabolism	2	1
Amino and metabolism	2	1

29 common DEGs were analyzed to confirm the mutated sites

There were 29 DEGs both in M1-vs-WT and M2-vs-WT comparisons, 15 of which were up-regulated and 14 of which were down-regulated in expression (Supplementary Table S4, Fig. 6A-6B). Among them, the expression of *PTTG_30094* in WT was 23.4- and 20.64-fold higher than that of M1 and M2, respectively, and the expression of *PTTG_01444* in WT was 10.67- and 6.88-fold higher than that of M1 and M2, respectively. Domain analysis was performed using Pfam software to elucidate biological functions, and their domains are related to the rare lipoprotein A (RlpA) like domain superfamily, the cytochrome P450 superfamily, the glycoside hydrolase superfamily, the major facilitator superfamily, and the phenylalanine ammonia-lyase superfamily.

EMS mutagenesis generates SNPs and Indels, thereby inducing base substitutions in the genome, and eventually leading to phenotype changes based on mutations. SNPs were screened by selecting only CG to TA mutations since mutations caused by EMS had the strong CG to TA transition bias. By mapping the Illumina reads of M1 and M2 to the reference genome, we identified 142 SNPs and 36 Indels from 29 DEGs both in M1-vs-WT and M2-vs-WT comparisons. The effects of SNPs were mainly missense (36.62%), in upstream regions (26.06%), in downstream regions (13.38%), synonymous mutations (11.97%), introns (5.64%), 3’-UTRs (2.11%), 5’-UTRs (2.11%), splice regions (1.41%), and stop gain (0.70%) variants (Fig. 6C). Since missense, splice variants and stop gain variants were predicted to have a moderate or high impact on the genome, those variants were regarded as mutations impacting gene functions. Similarly, Indels were mostly found in upstream (27.60%), intron (19.44%), downstream (11.11%) and splice acceptor (11.11%) regions (Fig. 6D). At the extreme, a 12-bp insertion and a 68-bp deletion were the largest Indels detected among the 29 DEGs containing Indels.

Effector candidates were identified from the 216 DEGs

In total, 30 effector candidates less than 300 amino acids were identified among the 216 proteins encoded by the DEGs using SignalP 5.0, TMHMM 2.0, Targetp 2.0, PredGPI (Table 2). 10 effector candidates were identified as cysteine-rich proteins with the percentage of cysteine greater than or equal to 3%. Pfam software analysis showed that PTTG_02997 has a Polysacc-deac-1 domain, and PTTG_04779 has a Thaumatin domain. Three effector motifs including [Y/F/W]xC, [L/I]xAR and G[I/F/Y][A/L/S/T]R were found in 30 effector candidates. However, no proteins containing the RxLR, YxSL[R/K] and [R/K]VY[L/I]R motifs were found.

Table 2
Characterization of 30 effector candidates of *Pt*.

Gene name	Protein ID	Start	End	AA[a]	Cys[b]	SPL%[c]	Pfam family	motif[d]
PTTG_25982	OAV97527.1	283774	284535	177	11	99.67		[Y/F/W]xC
PTTG_00528	OAV99683.1	1293484	1294592	245	5	98.61		
PTTG_05706	OAV91377.1	99128	100145	180	3	98.49		
PTTG_08504	OAV96694.1	959195	960977	261	9	98.50		
PTTG_11983	OAV96685.1	846080	847237	200	1	97.66		
PTTG_25529	OAV98838.1	843242	844456	165	12	99.87		[L/I]xAR
PTTG_25534	OAV98849.1	938968	940077	202	7	98.74		
PTTG_02944	OAV96672.1	803183	804937	242	4	99.80		[Y/F/W]xC
PTTG_02997	OAV95795.1	123092	124677	188	3	98.95	PF01522.21	[Y/F/W]xC
PTTG_04712	OAV91195.1	364128	365858	217	8	99.65		
PTTG_26199	OAV96956.1	706361	707112	181	7	99.35		[Y/F/W]xC
PTTG_26534	OAV95830.1	464431	465799	173	4	97.11	PF11937.8	[Y/F/W]xC
PTTG_04779	OAV95943.1	830568	832307	252	16	99.08	PF00314.17	[Y/F/W]xC [L/I]xAR
PTTG_07625	OAV97261.1	671834	672602	87	8	99.30		[Y/F/W]xC
PTTG_08990	OAV98722.1	1550599	1552165	200	4	99.50		
PTTG_27221	OAV93774.1	500716	501141	115	3	99.63		
PTTG_27510	OAV92868.1	376480	378161	227	1	95.97		
PTTG_04892	OAV95869.1	750867	752437	193	2	98.84		G[I/F/Y][A/L/S/T]R
PTTG_01155	OAV98136.1	1170869	1172267	98	1	99.88		
PTTG_03106	OAV94725.1	657164	658778	222	0	89.89		[L/I]xAR
PTTG_11858	OAV93820.1	182749	184468	235	3	94.09	PF01161.20	

[a]AA=Amino acid

[b]Cys=Cysteine residues

[c]SPL=signal peptide likelihood

[d]Motifs RxLR, YxSL[R/K], [L/I] xAR, [R/K]VY[L/I] R, G[I/F/Y][A/L/S/T]R and [Y/F/W]xC were searched for motifs in the effector candidates

*Effector candidiates for qRT-PCR and functional studies

Gene name	Protein ID	Start	End	AA[a]	Cys[b]	SPL%[c]	Pfam family	motif[d]
PTTG_06997	OAV89660.1	15529	16630	220	1	92.54		
PTTG_11662	OAV87798.1	22227	23882	235	1	82.77		
PTTG_25561	OAV98928.1	614656	615491	70	2	55.34		
*PTTG_27401**	OAV93118.1	90218	90912	211	12	99.68		
*PTTG_05290**	OAV98857.1	980461	981705	217	6	99.79		
*PTTG_27844**	OAV91894.1	362162	363027	127	6	99.80		[Y/F/W]xC
*PTTG_25521**	OAV98813.1	614656	615491	153	2	61.75		
*PTTG_26282**	OAV96625.1	282698	283700	251	3	92.38		[Y/F/W]xC
*PTTG_27224**	OAV93778.1	530795	531223	112	3	99.74		[Y/F/W]xC

[a]AA=Amino acid

[b]Cys=Cysteine residues

[c]SPL=signal peptide likelihood

[d]Motifs RxLR, YxSL[R/K], [L/I] xAR, [R/K]VY[L/I] R, G[I/F/Y][A/L/S/T]R and [Y/F/W]xC were searched for motifs in the effector candidates

*Effector candidiates for qRT-PCR and functional studies

The expression profiles of selected effector candidates were validated by qRT-PCR assay

We searched the data of *Pt* race PHTT(P) [28] and foundthat 6 of 30 effector candidates were differently expressed (Fig. 7A). So they were verified the expression levels of at different time post during *Pt* race PHNT infection by qRT-PCR analysis. The expression level of *PTTG_27844* at 0.5 days post-inoculation (dpi) was 3-fold higher than that of germ tubes (GT), 10-fold higher at 1 dpi, and increased to 304-fold higher at 4 dpi. The expression level of *PTTG_05290* at 0.5 dpi was 36-fold higher than that of GT, 28-fold higher at 1 dpi, and increased to 218-fold higher at 4 dpi. In addition, the expression patterns of *PTTG_27401* and *PTTG_25521* were similar to *PTTG_27844* and *PTTG_05290*, but the expression levels of *PTTG_27844* and *PTTG_25521* were lower. *PTTG_26282* expression peaked at 0.5 dpi and 4 dpi. *PTTG_27224* expression peaked at 0.5 dpi (Fig. 7B). These results were similar with the gene expression patterns predicted based on their FPKM values [28].

PTTG_27401 inhibition the progress of cell death (PCD) induced by BAX in *Nicotiana benthamiana*

To test whether the effector candidates could inhibit PCD, the coding regions of 6 effector candidates were separately cloned into a plant expression vector pEarleyGate103 (35S:Gene, T-DNA) (Supplementary Figure S3) and transiently expressed in *N. benthamiana* using *Agrobacterium* infiltration. The result showed, PTTG_27844,

PTTG_05290, PTTG_26282, PTTG_27224, and PTTG_25521 could not suppressed PCD triggered by the expression of *BAX* gene in tobacco leaves (Supplementary Figure S4). However, there was no necrosis at the sites where BAX and PTTG_27401 were infiltrated together, indicating that PTTG_27401 inhibited BAX action, preventing PCD from being induced, with potential toxic function (Fig. 8).

Discussion

It is well-known that mutation is the ultimate source of genetic variation, providing new alleles and genotypes [29]. The innovation of the present study is that we developed two *Lr19*-virulent mutants via EMS mutagenesis, M1 and M2, and confirmed that the mutation site only altered the virulence of *Pt* race PHNT to *Lr19*, but not other *Lr* genes, which benefits the screening of *AvrLr19* effector candidates.

RNA-seq has been extensively used to characterize transcriptional changes in both the host and pathogen at different stages of pathogen infection. Thus, it is possible to utilize transcriptomic data to identify DEGs during compatible and incompatible interactions. In this study, 216 DEGs including 29 DEGs found in both M1 and M2 were obtained, which suggested that they may play a certain role in infection of PHNT on TcLr19. PTTG_03515 is annotated as tyrosinase which can form melanin through a series of catalytic reactions. Melanin has been reported to play a role in the pathogenicity of fungi, and it is believed to contribute to fungal structure formation during infection, or to influence the host response to infection [30]. Another putative protein, PTTG_05196 is annotated as zinc finger protein that plays a role in pathogenic bacteria infection, and it has been proven that it can promote the occurrence of diseases [31].

30 effector candidates with certain criteria were identified. These genes provide valuable resources for screening *AvrLr19* candidates and pathogenesis-related genes. Among them, PTTG-01075 and PTTG-11895 are annotated as clan D glycoside hydrolases (GH-D), which are commonly referred to as plant cell wall degrading enzymes (PCWDEs) [32]. PTTG-12205 is annotated as a Major Facilitator Superfamily (MFS) of sugar transporters, which facilitates the transport of diverse molecules like sugars, vitamins, amino acids, hormones, etc. across cell membranes. MFS proteins might be relevant to the uptake of nutrients following the lysis of the host plant tissues, as well as the transport of toxins and antimicrobial compounds [33]. *PTTG_25982* was not only a common DEG in M1-vs-WT and M2-vs-WT comparisons, but was also predicted to be an effector candidate. Zhao et al sequenced *Pt* race PHTT(P) and analyzed the functional factors with conserved motifs [28], in this study, four common genes (*PTTG_25271*, *PTTG_04128*, *PTTG_08504*, and *PTTG_08503*) encoding PNPi like effectors were found.

Salcedo et al. [8] successfully cloned *AvrSr*35 and analyzed the expression patterns in wheat infected by wheat stem rust at 0, 1, 2 and 4 dpi, the results showed that *AvrSr*35 expression peaked at 4 dpi. In this study, we identified that PTTG_27401 suppressed PCD triggered by BAX and its expression peaked at 4 dpi. Further investigations on the molecular receptor of effector candidates should greatly improve our understanding of the avirulent mechanism of the *Pt*.

We profiled genes associated with the infection process of the *Lr19*-virulent mutants *Pt* strains derived from PHNT. By analyzing the transcriptomes of all samples, we found that the ratio of M1_sample 1, M1-sample 3, and M2-sample 6 to the reference genome were lower than other samples. It may be due to insufficient spores in the

sample. It was reported that 15 *Sr35*-virulent mutants generated by EMS were used to clone *AvrSr35* [8]. In the future, more *Lr19*-virulent mutants may need to be obtained in order to improve the power of this study. In addition, the function of *AvrLr19* candidates and pathogenesis-related genes of *Pt* will be identified by using the bacteria type III secretion system and host-induced gene silencing. By defining *AvrLr19* and its key functions, *AvrLr19* can be used to develop gene-specific molecular markers for directly monitoring *Pt* population changes in the field, which can be used for real-time monitoring of leaf rust races combined with marker-assisted selection (MAS) of wheat leaf rust resistance genes to predict the resistance of varieties and inform the correct use of resistant varieties. Our results provide valuable resources for identifying and characterizing *AvrLr19* effector candidates and pathogenic genes, and lay a foundation for further elucidating the pathogenic mechanism of *Pt* and analyzing the disease-resistance mechanism of *Lr19*.

Conclusion

In the present study, we obtained 2 *Lr19*-virulant mutant isolates developed by EMS mutagenesis of *Pt* race PHNT. By RNA-seq the WT isolate and the mutants M1 and M2, we aligned the sequences of the mutants with the wild-type isolate. We profiled genes associated with the infection process of the *Lr19*-virulent mutants Pt strains derived from PHNT. A total of 216 DEGs were found from M1-vs-WT, M2-vs-WT, and M1-vs-M2. Of these DEGs, 29 common DEGs were shared between M1-vs-WT and M2-vs-WT comparisons. Among the 216 DEGs encoding proteins, 30 were predicted to be effector candidates. Among them, 6 effector candidates were chosen and validated expression pattern and validated on tobacco, the results showed that PTTG_27401 could inhibit necrosis induced by BAX. Our results provide valuable resources for identifying and characterizing *AvrLr19* effector candidates and pathogenic genes, and lay a foundation for further elucidating the pathogenic mechanism of *Pt* and analyzing the disease-resistance mechanism of *Lr19*.

Methods

Plant materials and *Pt* isolates

Wheat seedlings of cultivar TcLr19 (Tc*6/RL6040), which is a near-isogenic line containing the *Lr19* gene, were requested from the Cereal Disease Lab of the USDA located at the University of Minnesota and were preserved in the *Pt* laboratory at Hebei Agricultural University. Wheat seedlings of cultivar Chinese Spring collected from our laboratory. Seedling plants of the all wheat cultivar were grown in a glasshouse. *Pt* pathotype 07-10-426-1 (PHNT race), collected from China and preserved in our laboratory, was used to inoculate wheat according to Roelfs' standards [34]. Seedlings (14 days old) from wheat lines Chinese Spring (*Lr19*-) inoculated by spraying with a suspension of *Pt* urediniospores were used as controls.

Staining and microscopic observation

To identify fungal tissues and the presence of dead cells in the leaf mesophyll of infected plants, the samples were stained via the Rohringer fluorescent staining method [35]. Stained tissues were observed under optical microscopy, and at least 10 fungal infection sites from three biological replicates were analyzed for each stained leaf sample.

EMS mutagenesis of *Pt* spores of the PHNT race

The *Lr19*-avirulent *Pt* race PHNT was used to create *Lr19*-virulent mutants by treatment with EMS as previously described [8]. Four different concentrations of EMS were used for mutagenesis: 0.1 M, 0.05 M, 0.01 M, and 0.005 M. After treated 2 hours with EMS, the germination rate of spores was observed using microscopy and unmodified *Pt* spores were used as control. Spores with at least 50% germination rate were inoculated on 12-day-old wheat TcLr19 seedlings. Inoculated seedlings were incubated in a dew chamber (22 °C) in dark conditions for 12 hours and then were kept in a growth chamber at 22 °C with a 16 h/8 h (day/ night) photoperiod.

Confirmation of mutation site

To ensure that the obtained *Lr19*-virulent mutant strains were not escapes of other rust strains and to validate that only *Lr19*-virulence was affected by EMS mutagenesis, the mutants and wild type leaf rust were analyzed by infecting a standard set of differential wheat near-isogenic lines that carry different *Lr* genes. Wheat seedlings of near-isogenic lines were requested from the Cereal Disease Lab of the USDA located at the University of Minnesota and were preserved in the *Pt* laboratory at Hebei Agricultural University. After 14 days, the phenotypes of hosts infected with wild-type and mutant strains were recorded according to Roelfs' 6-level (0, ;, 1, 2, 3, 4) classification method [34]. In addition, the molecular marker of *Lr19* was used to detect the validity of TcLr19 [27].

Transcriptome sequencing

Before sequencing, the *Pt* culture was purified by single-pustule isolation and pathotyped according to Roelfs' standards [34]. 14-day-old seedlings of TcLr19 inoculated with the urediniospores of the PHNT mutants were collected, and susceptible Chinese Spring wheat cultivar inoculated with the urediniospores of *Pt* race PHNT were used as a control. Plant samples were collected from severely diseased leaves at 14 dpi and three biological replicates were prepared for each group. Transcriptome sequencing and analyses were conducted by OE Biotech Co., Ltd. (Shanghai, China). Total RNA was extracted from the different samples and one microgram of high-quality total RNA was taken for RNA-seq library construction. The quantity and quality of extracted RNA were assessed using an Agilent 2100 Bioanalyzer (Agilent Technologies, UK). Sequencing was carried out on the Illumina HiSeqTM 2500 platform. Raw reads were processed using Trimmomatic [36] to obtain the clean reads. Then, the clean reads were mapped to reference genome "*Pt* 1–1 BBBD Race 1" [37] using Hisat2 [38] to obtain the location information on the reference genome or gene, as well as the specific sequence feature information of the sequenced sample. The FPKM values for each of the extracted transcripts were calculated using Cufflinks [39]. The read counts of each gene were obtained by HTSeq-count [40]. DEGs were identified using the DESeq (2012) R package [41]. "FDR-adjusted *p*-value < 0.05" and "|fold Change| >2" were set as the thresholds for significantly differential expression. Hierarchical clustering analysis of DEGs was performed to explore gene expression patterns. GO enrichment and KEGG [42] pathway enrichment analysis of DEGs were respectively performed using R based on the hypergeometric distribution.

Effector candidates among the 216 DEGs

To search for *Pt* effector candidates, we adopted the pipeline that shares common features with the effector prediction pipelines described for filamentous plant pathogens [43]. We first detected the presence of an N-terminal signal peptide through SignalP 5.0 [16], which indicates that candidates are presumed to have extracellular functions. Next, proteins with predicted sequences containing transmembrane helices were excluded from the set of predicted extracellular proteins using TMHMM 2.0 [18]. Subcellular localization signals was anlyzed by TargetP 2.0 [17]. The presence of a glycosylphosphatidylinositol (GPI) anchor was predicted using PredGPI [19] to identify proteins anchored to the membrane. Conserved protein domains were identified using

Pfam software [20]. Perl software was used to search for known motifs, including YxSL[R/K] [44] and RxLR [45] motif commonly detected in oomycetes, [L/I]xAR in some effector candidates of the rice blast pathogen, G[I/F/Y][A/L/S/T]R [46] in some effector candidates of flax rust, [Y/F/W]xC [47] and [R/K]VY[L/I]R [48] in the wheat powdery mildew fungi.

qRT-PCR analysis

Total RNA was extracted from infected leaves at 0.5, 1, 2, 4, 6, 8 and 14 dpi, samples collected from the GT of *Pt* uredospores served as a control. First-strand cDNA was synthesized from an equal amount of RNA using a PrimeScript Reverse Transcriptase kit (TaKaRa, Beijing, China). The *Pt β-actin* gene (GenBank accession OAV91054) was utilized as an internal reference gene, and 3 biological repeats were used in our experiments. The qRT-PCR reactions were conducted using a TransStart R Top Green qRT-PCR SuperMix (TransGen, Beijing, China) with a Roche-LightCycler 96 qRT-PCR instrument (Roche, Basel, Switzerland) using different primers designed according to different candidates (Supplementary Table S5). The transcriptional abundance of genes was quantitated relative to that of the *β-actin* following the $2^{-\Delta CT}$ method [49].

Transient expression assay in *N. benthamiana*

6 effector candidates without signal peptide were constructed into pEarleyGate103 with GFP tag by Gateway cloning [50]. The recombinant vector was transformed into *Agrobacterium tumefaciens* strain GV3101 using the freeze/thaw method [51]. *A. tumefaciens* mediated transient expression in *N. benthamiana* (seedlings of *N. benthamiana* were provided by our laboratory) was performed according to methods described previously [52]. The mammalian *BAX* gene (GenBank accession NP_031553) was used as positive control, and GFP as negative control. Leaves from 4–6-week-old seedling plants of *N. benthamiana* were initially infiltrated with *A. tumefaciens* transformants carrying different effector candidates, and then infiltrated with BAX at the same site 24 h later. A cell death phenotype was observed around 3–5 days postinoculation with effector candidates. For each of the effector candidates, this complete experiment was systemically repeated four times.

Abbreviations

Pt: *Puccinia triticina*; qRT-PCR: quantitative real-time PCR; dpi: days post-inoculation; EMS: ethyl methanesulfonate; WT: wild-type; DEGs: differentially expressed genes; GT: germ tubes; PCD: progress of cell death; HR: hypersensitive response; FPKM: the expected number of fragments per kilobase of transcript sequence per million base pairs; SNPs: single nucleotide polymorphisms; Indels: insertions and deletions; PCA: principal component analysis; GO: Gene Ontology; KEGG: Kyoto Encyclopedia of Genes and Genomes; GPI: glycosylphosphatidylinositol

Declarations

Acknowledgments

We say thanks to OE Biotech Co., Ltd. (Shanghai, China) for performance RNAseq and analyses.

Authors' Contributions

WW participated in developing and increasing urediniospores of the mutant isolates, data analyses, draft the manuscript. FF participated in analyzing and interpreting the data; FW and ZC participated in selecting isolate, producing spores, inoculating plants and virulence data analysis; XS, ZQ and BP bioinformatic analysis of RNAseq data; DD and HW conceived and coordinated the study, designed the experiments, provided materials and resources, interpreted data and revising the manuscript. All authors read and approved the final manuscript.

Funding

This work was supported by the Natural Science Foundation of Hebei (No. C2020204028) and National Natural Science Foundation of China (No. 31501623). The funding bodies played no role in the design of the study and collection, analysis, and interpretation of data and in writing the manuscript.

Availability of data and materials

The whole genome of the "*Pt* 1-1 BBBD Race 1" sequenced, assembled and annotated as previously reported[38], was used as a reference genome in this study. The datasets used and/or analysed during the current study are available from the corresponding author on reasonable request.

Ethics approval and consent to participate

Not applicable.

Consent for publication

Not applicable.

Competing interests

The authors declare that they have no competing interests.

Author details

[1]College of Plant Protection, Hebei Agricultural University / Technological Innovation Center for Biological Control of Crop Diseases and Insect Pests of Hebei Province, Baoding 071001, China. [2]Plant Protection Institute, Hebei Academy of Agricultural and Forestry Sciences, Baoding 071001, China.

References

1. Bolton MD, Kolmer JA, Garvin DF. Wheat leaf rust caused by *Puccinia triticina*. *Mol Plant Pathol*. *2008*;*9*(*5*):563–75.

2. Qureshi N, Bariana H, Kumran VV, Muruga S, Forrest KL, Hayden MJ, Bansal U. A new leaf rust resistance gene *Lr79* mapped in chromosome 3BL from durum wheat landrace Aus26582. Theor Appl Genet. 2018;131(5):1091–8.
3. Sarma D, Knott, DR. The transfer of leaf rust resistance from agropyron to triticum by irradiation. *Can J Genet Cytol. 1966;8(1)*:137–43.
4. Gupta SK, Charpe A, Prabhu KV, Haque MR. Identification and validation of molecular markers linked to the leaf rust resistance gene *Lr19* in wheat. *Theor Appl Genet. 2006;113(6)*:1027–36.
5. Saini RG, Kaur. Adult plant leaf rust (*Puccinia recondita tritici*) resistance of known *Lr* genes against three virulence variants of race 77 from Indian sub-continent. *Indian J Agr Sci. 1998;68(12)*:776–9.
6. Pink DAC. Strategies using genes for non-durable disease resistance. *Euphytica. 2002;124(2)*:227–236.
7. Reynolds MP, Calderini DF, Condon AG, Rajaram S. Physiological basis of yield gains in wheat associated with the *Lr19* translocation from agropyron elongatum. *Euphytica. 2001;119(1):139 – 44*.
8. Salcedo A, Rutter W, Wang S, Akhunova A, Bolus S, Chao S, Anderson N, Soto MFD, Rouse M, Szabo L, Bowden RL. Variation in the *AvrSr35* gene determines *Sr35* resistance against wheat stem rust race Ug99. *Science. 2017;358(6370):1604-6*.
9. Li Y, Xia C, Wang M, Yin C, Chen X. Whole-genome sequencing of *Puccinia striiformis* f. sp. *tritici* mutant isolates identifies avirulence gene candidates. *BMC Genomics. 2020;21*(1):247–69.
10. Garnica DP, Upadhyaya NM, Dodds PN, Rathjen JP. Strategies for wheat stripe rust pathogenicity identified by transcriptome sequencing. PLoS One. 2013;8(6):e67150.
11. Wei J, Cui L, Zhang N, Du D, Meng Q, Yan H, Liu D, Yang W. *Puccinia triticina* pathotypes THTT and THTS display complex transcript profiles on wheat cultivar Thatcher. *BMC genetics. 2020;21(1)*:48–59.
12. Elmore MG, Banerjee S, Pedley KF, Ruck A, Whitham SA. De novo transcriptome of phakopsora pachyrhizi uncovers putative effector repertoire during infection. *Physiol Mol Plant Pathol. 2020;110*:101464–101473.
13. Rutter WB, Salcedo A, Akhunova A, He F, Wang S, Liang H, Bowden RL, Akhunov E. Divergent and convergent modes of interaction between wheat and *Puccinia graminis* f. sp. *tritici* isolates revealed by the comparative gene co-expression network and genome analyses. BMC Genom. 2017;18(1):291–311.
14. Flor HH. Current status of the gene-for-gene concept. *Annu Rev Phytopathol. 2003;9:275–296*.
15. Jones JD, Dangl JL. The plant immune system. *Nature. 2006;444(7117):323–9*.
16. Almagro Armenteros JJ, Tsirigos KD, Sonderby CK, Petersen TN, Winther O, Brunak S, Heijne GV, Nielson H. SignalP 5.0 improves signal peptide predictions using deep neural networks. *Nat Biotechnol. 2019;37(4):420–3*.
17. Emanuelsson O, Nielsen H, Brunak S, Heijne GV. Predicting subcellular localization of proteins based on their N-terminal amino acid sequence. *J Mol Biol. 2000;300(4):1005–16*.
18. Krogh A, Larsson B, von Heijne G, Sonnhammer EL. Predicting transmembrane protein topology with a hidden Markov model: application to complete genomes. *J Mol Biol. 2001;305(3):567 – 80*.
19. Pierleoni A, Martelli PL, Casadio R. PredGPI: a GPI anchor predictor. *BMC Bioinformatics. 2008;9:392–403*.
20. Finn RD, Bateman A, Clements J, Coggill P, Eberhardt RY, Eddy SR, Heger A, Hetherington K, Holm L, Mistry J, Sonnhammer ELL, Tate J, Punte M. Pfam: the protein families database. *Nucleic Acids Res. 2014;42:D222–30*.

21. Anderson C, Khan MA, Catanzariti AM, Jack CA, Nemri A, Lawrence GJ, Upadhyaya NM, Hardham AR, Ellis JG, Dodds PN, Jones DA. Genome analysis and avirulence gene cloning using a high-density RADseq linkage map of the flax rust fungus, Melampsora lini. *BMC Genomics*. *2016*;*17*(*1*):*667 – 87*.
22. Kemen E, Kemen AC, Rafiqi M, Hempel U, Mendgen K, Hahn M, Voegele RT. Identification of a protein from rust fungi transferred from haustoria into infected plant cells. *Mol Plant-Microb Interact. 2005*;*18*(*11*):*1130-9*.
23. Petre B, Joly DL, Duplessis S. Effector proteins of rust fungi. *Front Plant Sci*. *2014*;*5*(*5*):416–22.
24. Chen J, Upadhyaya NM, Ortiz D, Sperschneider J, Li F, Bouton C, Breen S, Dong C, Xu B, Zhang X, Mago R, Newell K, Xia X, Bernoux M, Taylor JM, Steffenson B, Jin Y, Zhang P, Kanyuka K, Figueroa M, Ellis JG, Park RF, Dodds PN. Loss of *AvrSr50* by somatic exchange in stem rust leads to virulence for *Sr50* resistance in wheat. *Science*. *2017*;*358*(*6370*):1607–10.
25. Segovia V, Bruce M, Rupp JL, Huang L, Bakkeren G, Trick HN, Fellers JP. Two small secreted proteins from induce reduction of ß-glucoronidase transient expression in wheat isolines containing and *Lr9*, *Lr24* and *Lr26*. Can J Plant Pathol. *2016*;38(1):91–102.
26. Wu JQ, Sakthikumar S, Dong C, Zhang P, Cuomo CA, Park RF. Comparative genomics integrated with association analysis identifies candidate effector genes corresponding to *Lr20* in phenotype-paired *Puccinia triticina* isolates from Australia. *Front Plant Sci*. *2017*;*8*:148–66.
27. Shan X, Blake TK, Talbert LE. Conversion of AFLP markers to sequence-specific PCR markers in barley and wheat. *Theor Appl Genet*. *1999*;*98*(*6–7*):1072–8.
28. Zhao S, Shang X, Bi W, Yu X, Liu D, Kang Z, Wang X, Wang X. Genome-wide identification of effector candidates with conserved motifs from the wheat leaf rust fungus puccinia triticina. *Front Microbiol*. *2020*;*11*:*1188 – 203*.
29. McDonald BA, Linde C. Pathogen population genetics, evolutionary potential, and durable resistance. Annu Rev Phytopathol. 2002;40:349–79.
30. Elliott CE, Callahan DL, Schwenk D, Nett M, Hoffmeister D, Howlett BJ. A gene cluster responsible for biosynthesis of phomenoic acid in the plant pathogenic fungus, Leptosphaeria maculans. *Fungal Genet Biol*. *2013*;*53*:*50 – 8*.
31. Comijn J, Berx G, Vermassen P, Verschueren K, van Grunsven L, Bruyneel E, Mareel M, Huylebroeck D, van Roy F. The two-handed E box binding zinc finger protein SIP1 downregulates E-cadherin and induces invasion. *Mol Cell*. *2001*;*7*(*6*):1267–78.
32. Okazawa Y, Miyazaki T, Yokoi G, Ishizaki Y, Nishikawa A, Tonozuka T. Crystal structure and mutational analysis of isomalto-dextranase, a member of glycoside hydrolase family 27. *J Biol Chem*. *2015*;*290*(*43*):*26339-49*.
33. Patil SS, Prashant R, Kadoo NY, Upadhyay A, Gupta VS. Global study of MFS superfamily transporters in arabidopsis and grapes reveals their functional diversity in plants. *Plant Gene*. 2019;*18*.
34. Roelfs AP. Race specificity and methods of study. Cereal Rusts. 1984;a4(2):131–64.
35. Rohringer R. Calcofluor. An optical brightener for fluorescence microscopy of fungal plant parasites in leaves. Phytopathology. *1977*;77(6):808–10.
36. Bolger AM, Lohse M, Usadel B. Trimmomatic: a flexible trimmer for Illumina sequence data. Bioinformatics. 2014;30(15):2114–20.

37. Kiran K, Rawal HC, Dubey H, Jaswal R, Devanna BN, Gupta DK, Bhardwaj SC, Prasad P, Pal D, Chhuneja P, Balasubramanian P, Kumar J, Swami M, Solanke AU, Gaikwad K, Singh NK, Sharma TR. Draft genome of the wheat rust pathogen (*Puccinia triticina*) unravels genome-wide structural variations during evolution. Genome Biol Evol. 2016;8(9):2702–21.
38. Kim D, Langmead B, Salzberg SL. HISAT: a fast spliced aligner with low memory requirements. *Nat Methods*. *2015*;*12*(*4*):357–60.
39. Trapnell C, Williams BA, Pertea G, Mortazavi A, Kwan G, van Baren MJ, Salzberg SL, Wold BJ, Pachter L. Transcript assembly and quantification by RNASeq reveals unannotated transcripts and isoform switching during cell differentiation. *Nat Biotechnol*. *2010*;*28*(*5*):511–5.
40. Anders S, Pyl PT, Huber W. HTSeq–a Python framework to work with high-throughput sequencing data. *Bioinformatics. 2015*;*31*(*2*):166–9.
41. Anders S, Huber W. Differential expression of RNA-Seq data at the gene level – the DESeq package. *EMBL*. 2013.
42. Kanehisa M, Araki M, Goto S, Hattori M, Hirakawa M, Itoh M, Katayama T, Kawashima S, Okuda S, Tokimatsu T, Yamanishi Y. KEGG for linking genomes to life and the environment. Nucleic Acids Res. 2008;36:D480-4.
43. Haddadi P, Ma L, Wang H, Borhan MH. Genome-wide transcriptomic analyses provide insights into the lifestyle transition and effector repertoire of Leptosphaeria maculans during the colonization of Brassica napus seedlings. Mol Plant Pathol. 2016;17(8):1196–210.
44. Lévesque CA, Brouwer H, Cano L, Hamilton JP, Holt C, Huitema E, Raffaele S, Robideau GR, Thines M, Win J, Zerillo MM, Beakes GW, Boore JL, Busam D, Dumas B, Ferriera S, Fuerstenberg SI, Gachon CMM, Gaulin E, Govers F, Grenville-Briggs L, Horner N, Hostetler J, Jiang RHY, Johnson J, Krajaejun T, Lin H, Meijer HJG, Moore B, Morris P, Phuntmart V, Puiu D, Shetty J, Stajich JE, Tripathy E, Wawra S, van West P, Whitty BR, Coutinho PM, Henrissat E, Martin F, Thomas PD, Tyler BM, Vries RPD, Kamoun S, Yandell M, Tisserat N, Buell CR. Genome sequence of the necrotrophic plant pathogen *Pythium ultimum* reveals original pathogenicity mechanisms and effector repertoire. Genome Biol. 2010;11(7):R73–95.
45. Whisson SC, Boevink PC, Moleleki L, Avrova AO, Morales JG, Gilroy EM, Armstrong MR, Grouffaud S, van West P, Chapman S, Hein I, Toth LK, Pritchard L, Birch PRJ. A translocation signal for delivery of oomycete effector proteins into host plant cells. Nature. 2007;450(7166):115–8.
46. Catanzariti AM, Dodds PN, Lawrence GJ, Ayliffe MA, Ellis JG. Haustorially expressed secreted proteins from flax rust are highly enriched for avirulence elicitors. Plant Cell. 2006;18(1):243–56.
47. Godfrey D, Böhlenius H, Pedersen C, Zhang Z, Emmersen J, ThordalChristensen H. Powdery mildew fungal effector candidates share N-terminal Y/F/WxC-motif. BMC Genom. 2010;11:317–30.
48. Ridout CJ, Skamnioti P, Porritt O, Sacristan S, Jones JD, Brown JK. Multiple avirulence paralogues in cereal powdery mildew fungi may contribute to parasite fitness and defeat of plant resistance. *Plant Cell*. *2006*;*18*(*9*):*2402–14*.
49. Schmittgen TD, Livak KJ. Analyzing real-time PCR data by the comparative C T method. *Nat Protoc*. *2008*;*3*(*6*):*1101-8*.
50. Wang F, Yuan S, Wu W, Yang Y, Cui Z, Wang H, Liu D. TaTLP1 interacts with TaPR1 to contribute to wheat defense responses to leaf rust fungus. *PLoS Genet*. *2020*;*16*(*7*):*e1008713*.
51. Wise AA, Liu Z, Binns AN. Three methods for the introduction of foreign DNA into agrobacterium. Methods Mol Biol. 2006;343:43–53.

52. Ma L, Lukasik E, Gawehns F, Takken FLW. The use of agroinfiltration for transient expression of plant resistance and fungal effector proteins in *Nicotiana benthamiana* leaves. *Methods Mol Biology*. *2012*;*835*:61–74.

Figures

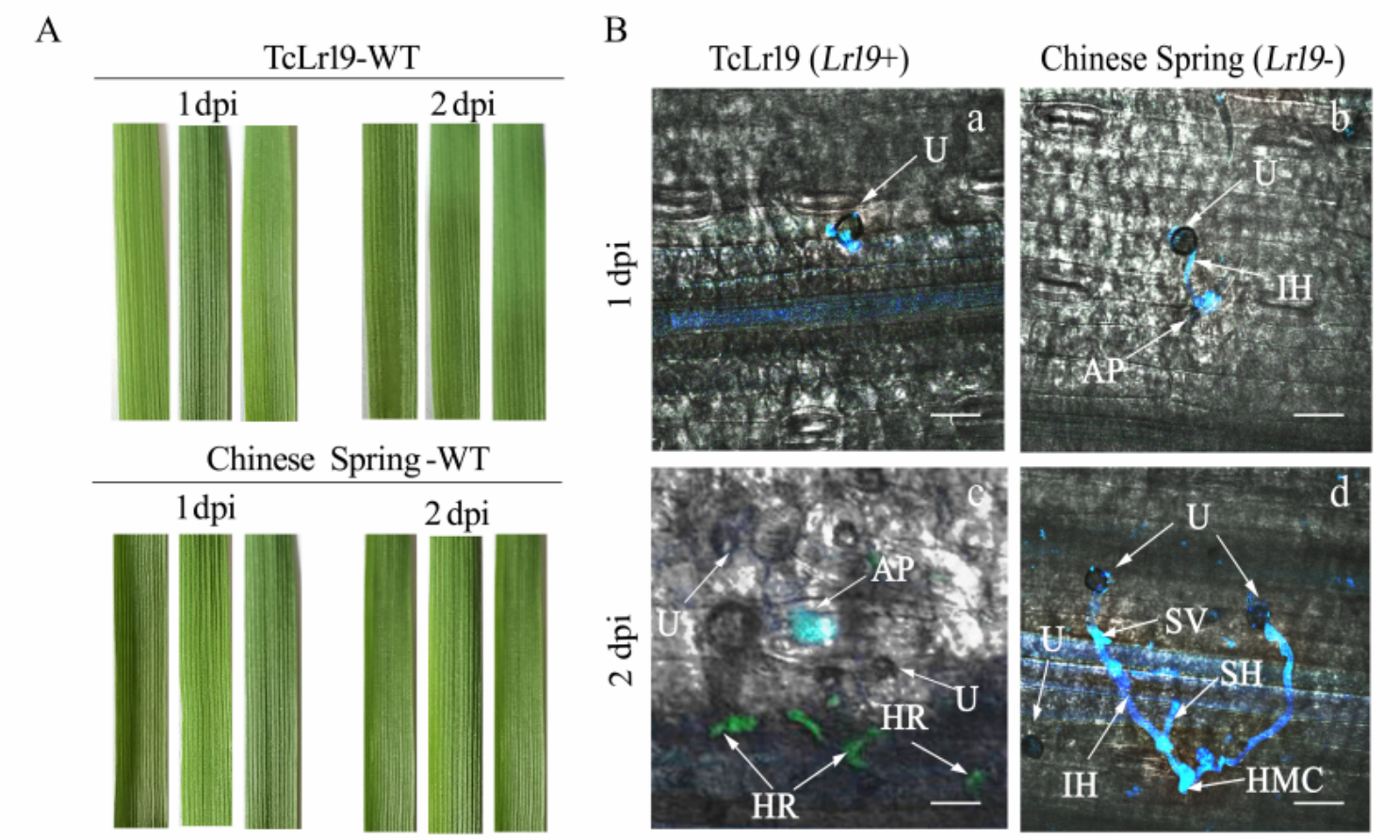

Figure 1

Lr19 provides prehaustoria resistance against Pt. Infected leaves of susceptible cultivar Chinese Spring (Lr19-) and resistant line TcLr19 (Lr19+) were collected at 1- and 2-days post inoculation (dpi). (a and b) Fungal infection hyphae (IH) (stained blue) entered the leaf mesophyll tissue (stained blue) through the plant stoma (S) in both wheat lines at 1 dpi. Fungal haustoria (H) developed only in susceptible Chinese Spring (b). (c and d) Imaging at 2 dpi revealed fungal growth in susceptible Chinese Spring (d) but no further fungal growth in TcLr19 (c). At 2 dpi revealed presumably dead host cells (stained green) in TcLr19 (c); no dead cells were revealed in Chinese Spring (d). IH: infection hypha; HMC: haustorial mother cell; SH: second hypha; HR: hypersensitive response; U: spores; SV: substomatal vesicle; Ap, appressorium. Scale bar, 50 μm.

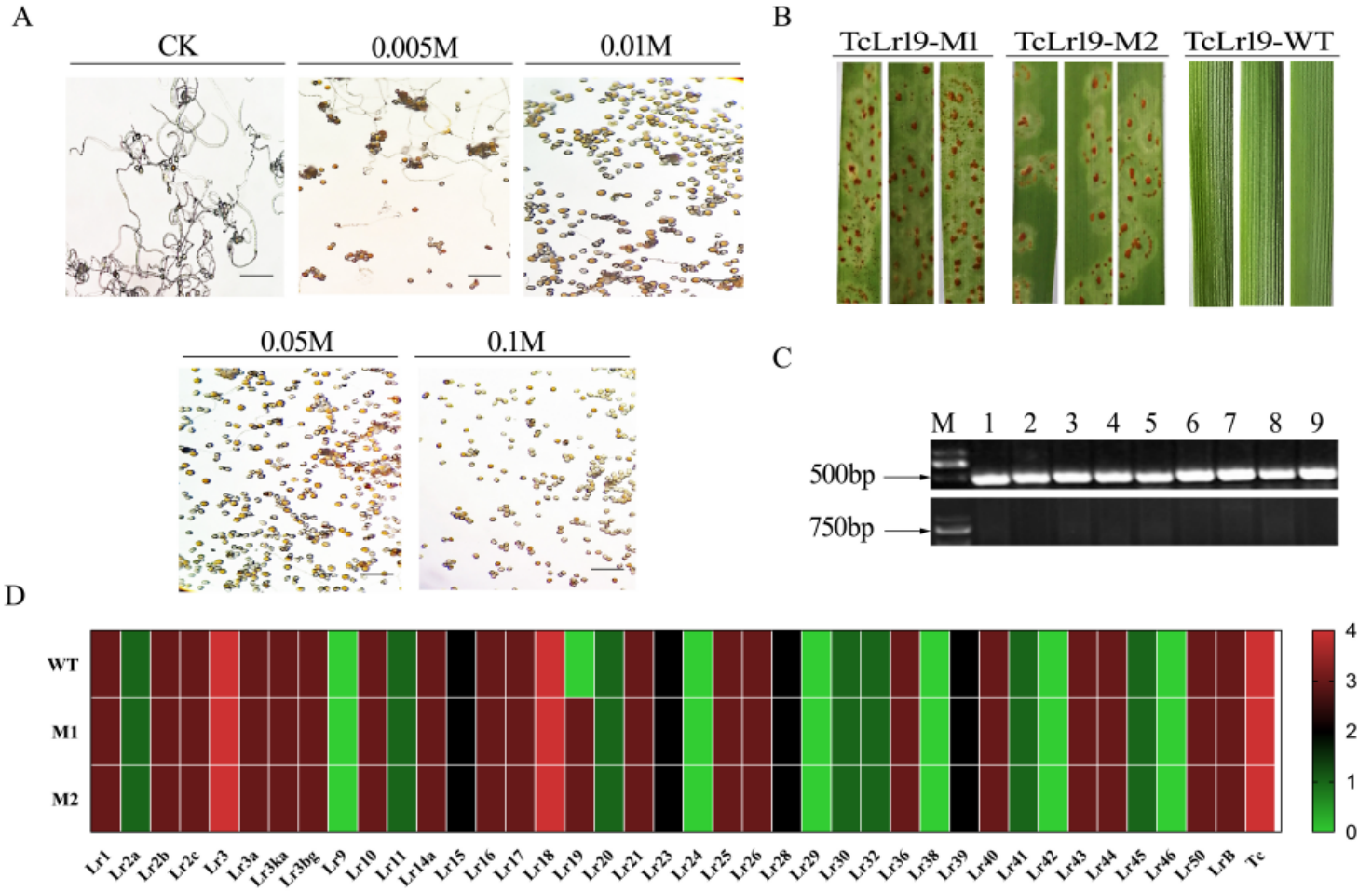

Figure 2

Lr19- virulent Mutants were obtained and confirmed. (A) The germination rate of Pt spores of PHNT race under different EMS concentration; (B) The phenotypes of Lr19- virulent Mutants M1 and M2 were compared with wild-type (WT); (C) Molecular markers detection of Lr19. There was a specific band at 500 bp for forward primer detection and there was no specific band at 750 bp for reverse primer detection, M is the abbreviation of marker, 1-9 represents 9 test samples. (D) Heatmap of WT and its mutants (M1 and M2) of Pt based on infection types, the virulence characterization of all isolates was conducted on the 39 wheat Lr single-gene differentials, ITs 0 to 4 were transformed to the color key ranging from green to red, which indicate avirulent (resistant) to virulent (susceptible) reactions.

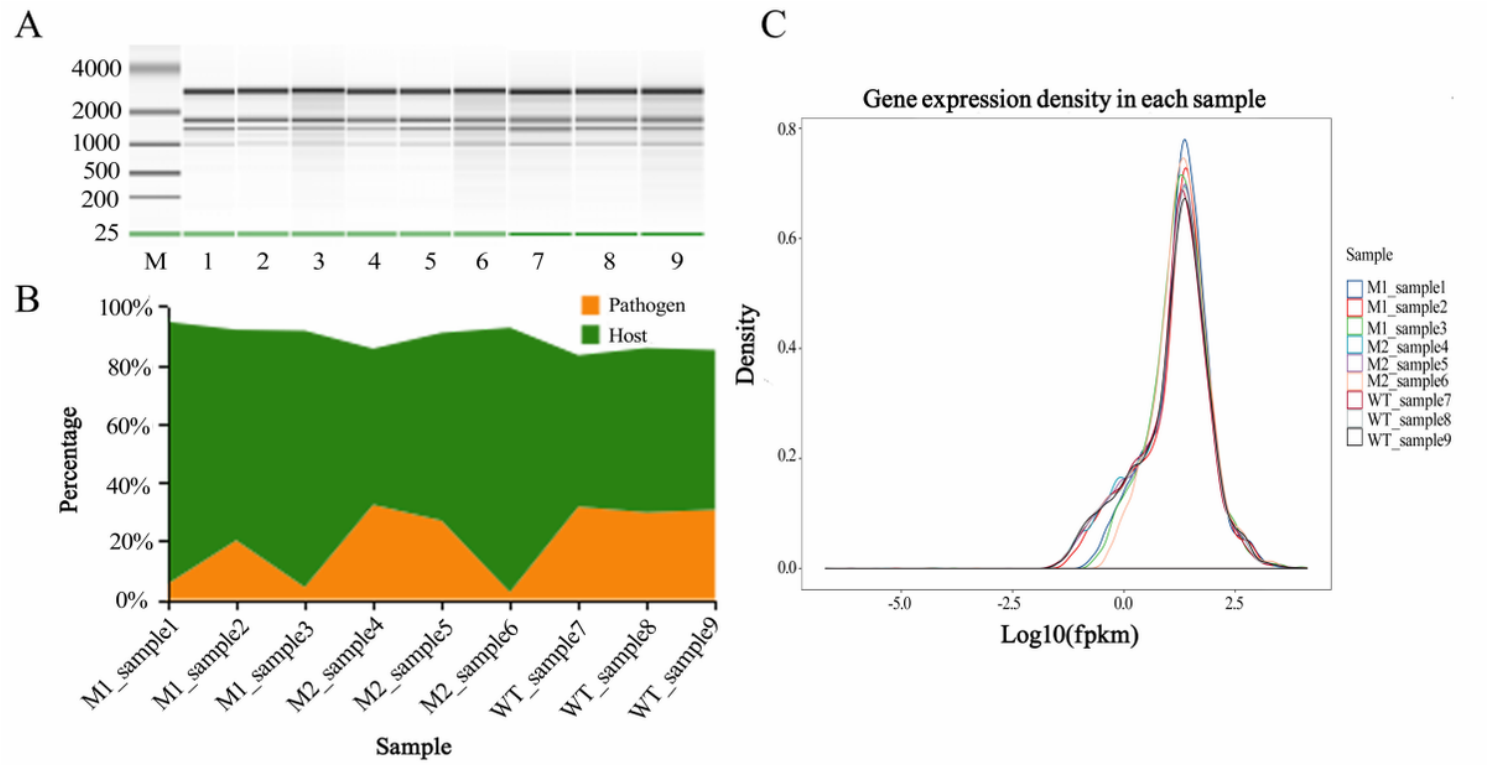

Figure 3

Lr19- virulent Mutants were obtained and confirmed. (A) The germination rate of Pt spores of PHNT race under different EMS concentration; (B) The phenotypes of Lr19- virulent Mutants M1 and M2 were compared with wild-type (WT); (C) Molecular markers detection of Lr19. There was a specific band at 500 bp for forward primer detection and there was no specific band at 750 bp for reverse primer detection, M is the abbreviation of marker, 1-9 represents 9 test samples. (D) Heatmap of WT and its mutants (M1 and M2) of Pt based on infection types, the virulence characterization of all isolates was conducted on the 39 wheat Lr single-gene differentials, ITs 0 to 4 were transformed to the color key ranging from green to red, which indicate avirulent (resistant) to virulent (susceptible) reactions.

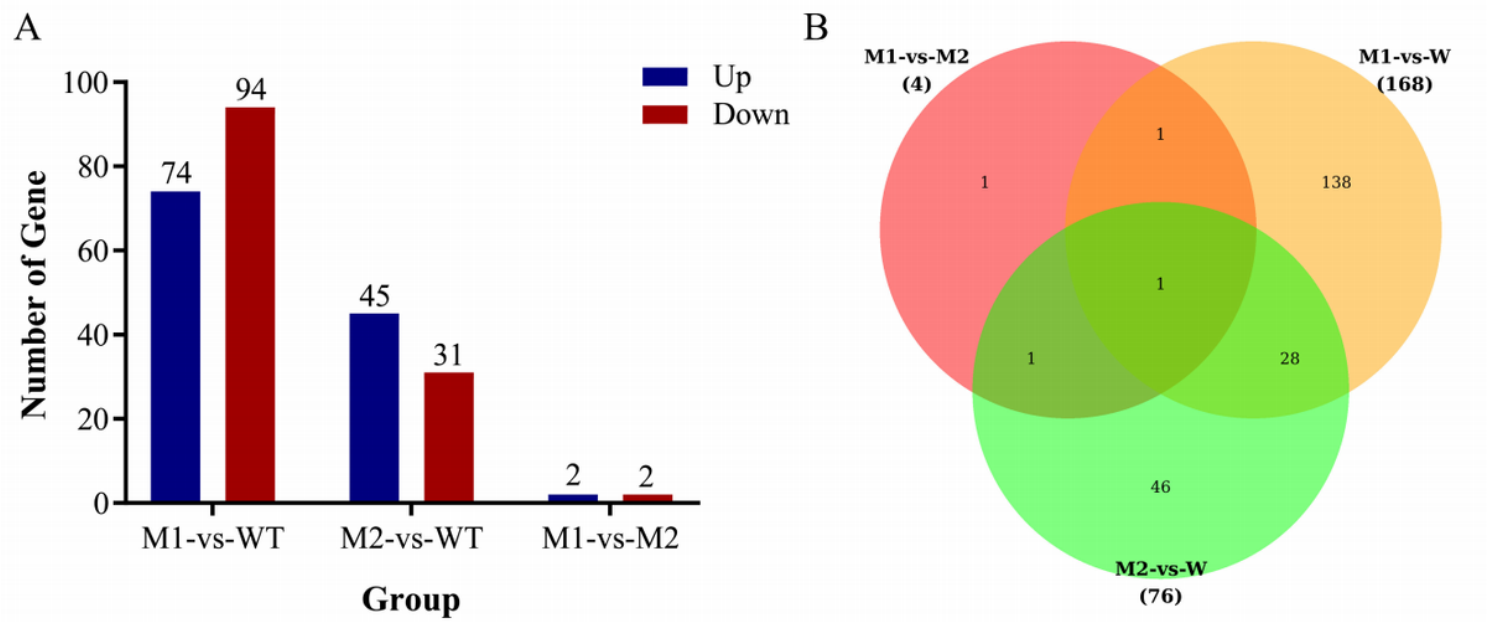

Figure 4

The differentially expressed genes (DEGs). (A) Number of up-regulated and down regulated DEGs in different samples; (B) DEGs that are unique or shared among various samples comparisons in mutants (M1M2) and WT. The numbers of DEGs are noted in each section of the Venn diagrams.

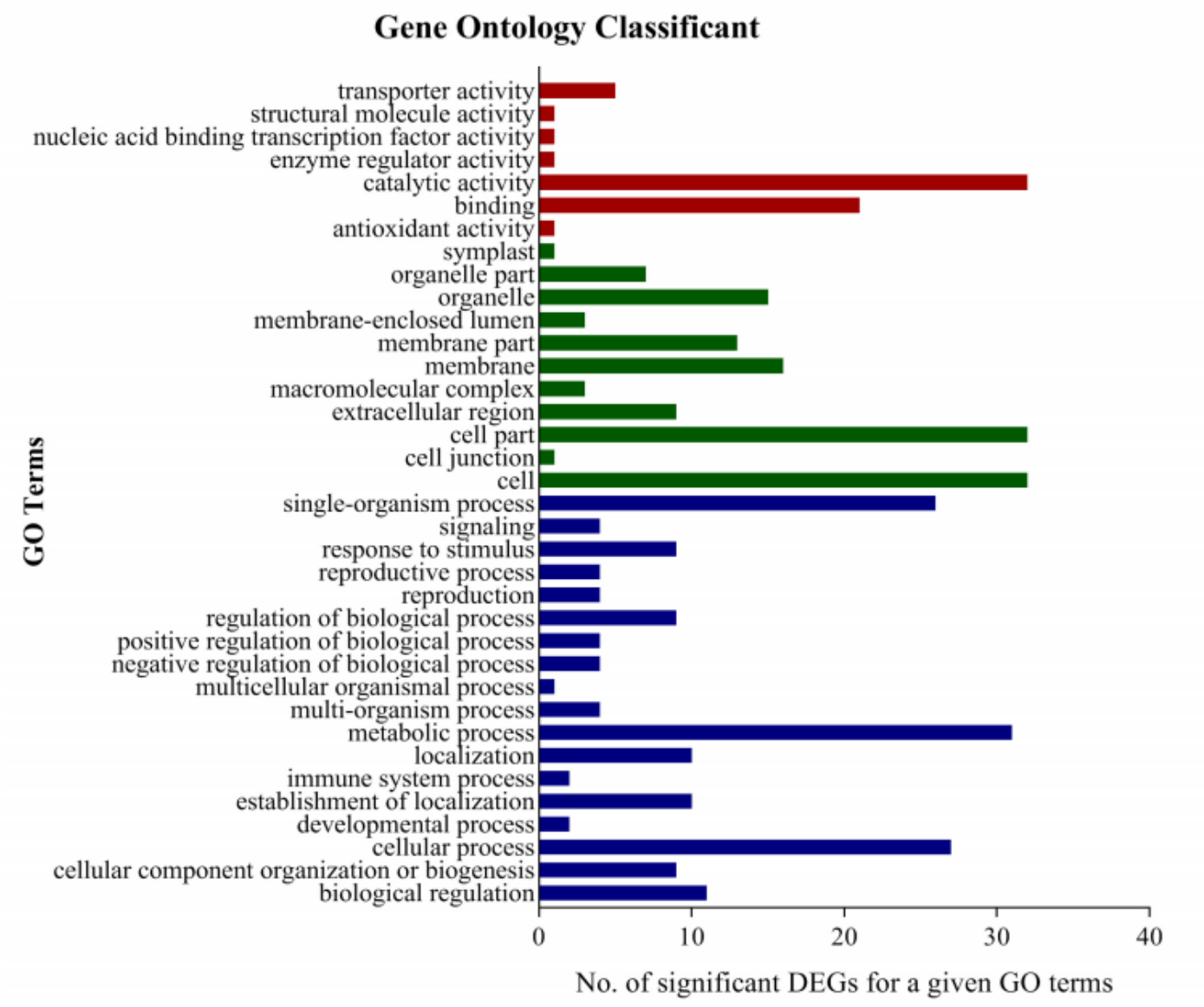

Figure 5

Bar graph showing the number of 216 DEGs identified utilizing gene ontology (GO) enrichment analysis for involvement in specific molecular function, cellular component and biological processes. In the figure, red color represents molecular function, green color represents molecular function, blue color represents molecular function, the Y coordinate is the name of GO term, and the X coordinate is number of gene.

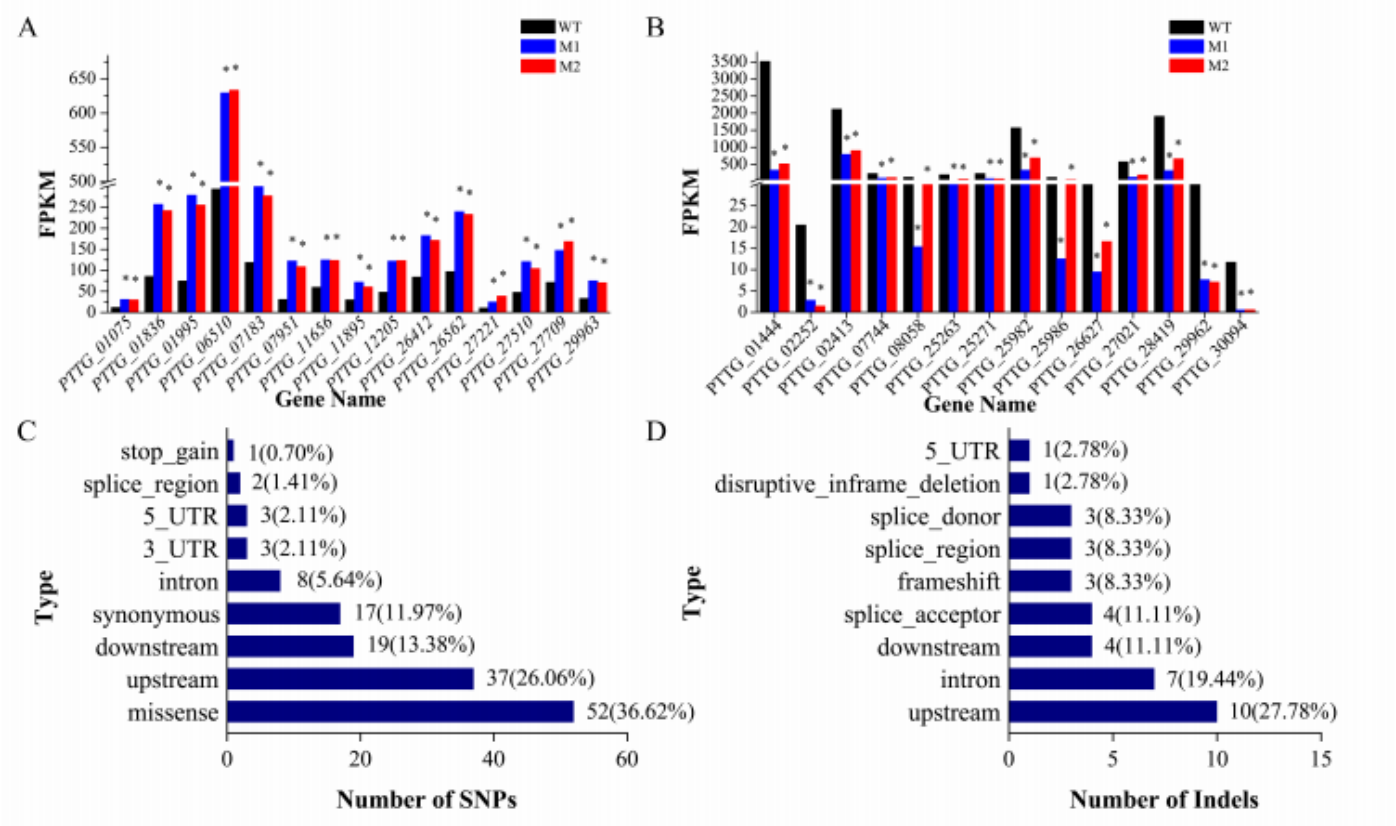

Figure 6

29 common DEGs between the M1-vs-WT and M2-vs-WT. (A, B) directly reflect the expression amount and difference multiple of genes in M1, M2 and WT. (A) 15 up-regulated DEGs; (B) 14 down-regulated DEGs. (C, D) Types and frequencies of SNPs/ Indels effects detected from the 29 DEGs. The number and percentage of all EMS-induced SNPs/ Indels for each 29 DEGs. 5_UTR is the acronym of 5_UTR premature start codon gain variant. (C) Types and frequencies of SNPs effects detected from the 29 DEGs. (D) Types and frequencies of Indels effects detected from the 29 DEGs.

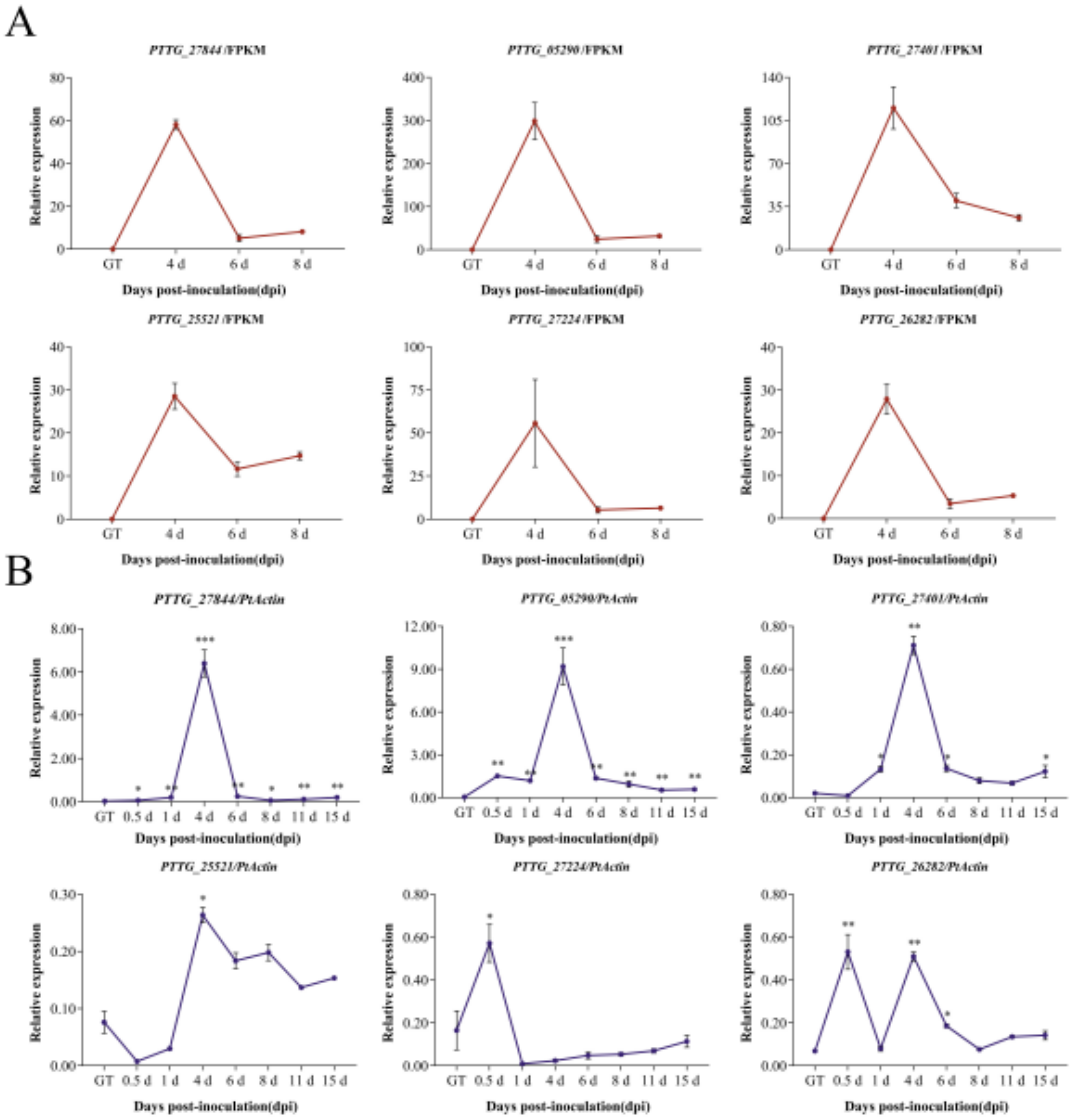

Figure 7

Transcriptional profile of genes during the Pt pathotypes infection measured by qRT-PCR. The transcript levels of the six selected effector candidates during Pt infection at 0.5, 1, 4, 6, 8, 11, and 15 dpi were determined by qRT-PCR assay. Samples collected from the GT of Pt uredospores served as a control. The transcript levels for all genes were expressed as linearized fold-PtActin levels, which were calculated according to the formula 2△CT. Data were expressed as mean values ± SE from 3 biological replicates. An asterisk (*P < 0.05,**P < 0.01, ***P <0.001) indicates a significant difference between the control and infection samples by Dunnett' s test.

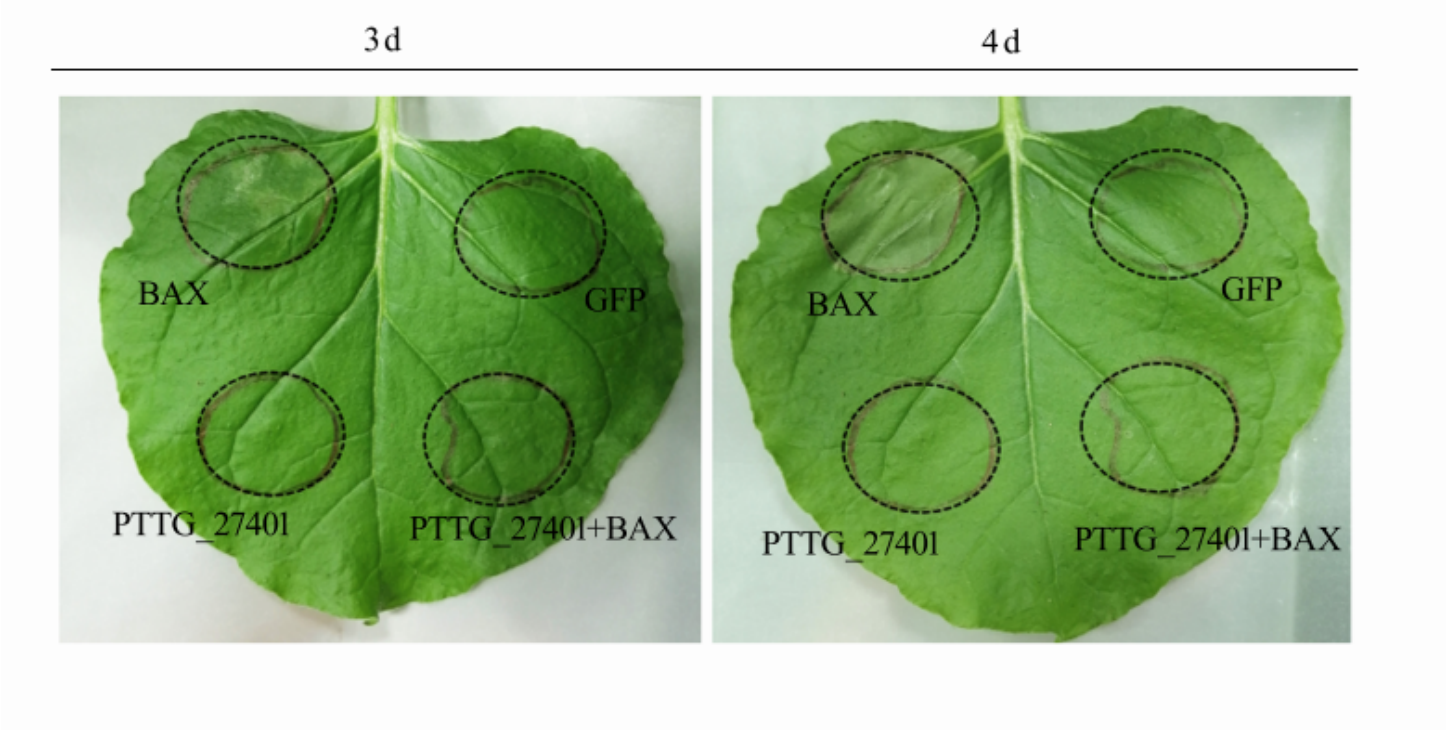

Figure 8

PTTG_27401 could inhibit PCD induced by BAX in N.benthamiana. The PTTG_24701 inhibit the cell death triggered by BAX was observed on 3 day and 4 day, we can see the area change PCD induced by BAX.

Supplementary Files

This is a list of supplementary files associated with this preprint. Click to download.

- Additionalfile1.docx
- Additionalfile3.xls
- Additionalfile2.docx